Bioactive Materials 6 (2021) 2535–2545

Contents lists available at ScienceDirect

Bioactive Materials

journal homepage: www.sciencedirect.com/journal/bioactive-materials

Self-adhesive lubricated coating for enhanced bacterial resistance

Ying Han [a,1], Weiwei Zhao [a,1], Yiwei Zheng [a], Haimang Wang [a], Yulong Sun [a], Yifei Zhang [b], Jing Luo [c], Hongyu Zhang [a,*]

[a] State Key Laboratory of Tribology, Department of Mechanical Engineering, Tsinghua University, Beijing, 100084, China
[b] Central Laboratory, Peking University School and Hospital of Stomatology, Beijing, 100081, China
[c] Beijing Research Institute of Automation for Machinery Industry Co., Ltd, Beijing, 100120, China

ARTICLE INFO

Keywords:
Dopamine
Lubrication
Biomimetic coating
Bacterial resistance
Self-adhesive

ABSTRACT

Limited surface lubrication and bacterial biofilm formation pose great challenges to biomedical implants. Although hydrophilic lubricated coatings and bacterial resistance coatings have been reported, the harsh and tedious synthesis greatly compromises their application, and more importantly, the bacterial resistance property has seldom been investigated in combination with the lubrication property. In this study, bioinspired by the performances of mussel and articular cartilage, we successfully synthesized self-adhesive lubricated coating and simultaneously achieved optimal lubrication and bacterial resistance properties. Additionally, we reported the mechanism of bacterial resistance on the nanoscale by studying the adhesion interactions between biomimetic coating and hydrophilic/hydrophobic tip or living bacteria via atomic force microscopy. In summary, the self-adhesive lubricated coating can effectively enhance lubrication and bacterial resistance performances based on hydration lubrication and hydration repulsion, and represent a universal and facial strategy for surface functionalization of biomedical implants.

1. Introduction

The two key challenges associated with biomedical implants are limited surface lubrication and bacterial biofilm formation, which can induce serious tissue damage and a series of consecutive complications [1]. Despite the development of lubricated coatings [2,3] and anti-bacterial coatings (containing bacterial resistance materials [4,5] and bactericidal materials [6,7]) in recent years, the lubrication and bacterial resistance properties of the biomedical implants have failed to combine well in previous studies. Accordingly, it is particularly meaningful to design an innovative method for surface functionalization that considers both enhanced lubrication and bacterial resistance performances.

In nature, super-lubricated system, typically the articular cartilage in a healthy joint, performs an extremely low coefficient of friction (COF, 0.001–0.03) [8,9]. It has been reported by Klein et al. that articular cartilage attains low COF owing to the hydration lubrication mechanism of charged phosphatidylcholine lipids [10], which can tightly attract many water molecules to form a tenacious hydration layer. Specifically, when subjected to shear force, the hydration layer can respond in a fluidlike manner to minimize drag and thus result in a small COF. Inspired by this mechanism, zwitterionic polymers that biomimick charged phosphatidylcholine lipids in articular cartilage, such as poly (2-methacryloxyethyl phosphorylcholine) (PMPC), have been widely investigated for enhancing lubrication [11–14]. However, the harsh and tedious synthesis, and more importantly, the stability of these lubricated coatings greatly limit their clinical applications.

On the other hand, infection of biomedical implants is generally caused by the formation of a bacterial biofilm, which is initiated due to the reversible bacterial adhesion on the surface [15,16]. The bacteria contain different proteinaceous extracellular appendages [17–20] that contribute to adhesion directly or indirectly [21]. Therefore, inhibiting the initial adhesion of protein and bacteria is the key to prevent biofilm formation. Previous studies have shown that surface modification of PMPC or other zwitterionic polymers is an effective way to protect the substrate from protein adsorption [22,23] and bacterial adhesion [24–26]. Basically, it is not energetically feasible for the protein and bacteria to replace the hydration layer formed on the superficial surface

Peer review under responsibility of KeAi Communications Co., Ltd.
* Corresponding author.
E-mail address: zhanghyu@tsinghua.edu.cn (H. Zhang).
[1] These authors contributed equally to this work.

https://doi.org/10.1016/j.bioactmat.2021.01.028
Received 19 November 2020; Received in revised form 6 January 2021; Accepted 22 January 2021

of the substrate. However, the anti-adhesion mechanism has seldom been deeply reported on the nanoscale, especially in combination with the lubrication property.

In our previous studies [27,28], we successfully synthesized a self-adhesive copolymer material (DMA-MPC) using dopamine methacrylamide (DMA) and MPC via free radial polymerization, and preliminarily reported the bacterial resistance property [29]. Here, we aimed to generate a stable biomimetic coating and explore the lubrication and bacterial resistance performances on both the macroscale and the nanoscale (Fig. 1). Consequently, dopamine-assisted codeposition with the DMA-MPC copolymer (PDA/DMA-MPC) was used in this study [30–32]. Dopamine acted as an anchoring and intercalated agent to facilitate the progressive assembly of multi-layered coating. Furthermore, we investigated the interactions between the as-fabricated lubricated coating and the representative hydrophilic/hydrophobic tip or living bacteria by atomic force microscopy (AFM) under force measurement, which was a universal method for the examination of surface−surface interactions [33–36]. It was hypothesized that the biomimetic coating developed herein could not only effectively enhance lubrication property based on hydration lubrication, but also achieve excellent bacterial resistance owing to hydration repulsion [37].

2. Materials and methods

2.1. Materials

High purity titanium alloy (Ti6Al4V, 99%) sheet was purchased from Goodfellow Cambridge Ltd., Huntingdon, UK. Dopamine hydrochloride, sodium tetraborate, methacrylic anhydride, deuterium solvent and *tert*-butyl hydroperoxide (TBHP) were purchased from J&K Scientific Ltd., Beijing, China. Azodiisobutyronitrile (AIBN), Tris-HCl buffer and polystyrene (PS) microspheres were purchased from Aladdin Bio-Chem Technology Co., Ltd., Shanghai, China. 2-Methacryloxyethyl phosphorylcholine (MPC) was purchased by Joy-Nature Co., Nanjing, China.

2.2. Synthesis of DMA-MPC copolymer

Dopamine methacrylamide (DMA) was synthesized based on the following procedures. Dopamine hydrochloride (5 g), sodium tetraborate (10 g) and sodium bicarbonate (4 g) were dissolved in deionized water (100 mL) under N_2 atmosphere. Methacrylic anhydride (5 mL) was dissolved in tetrahydrofuran (25 mL) and then added dropwise to the above solution (pH = 8). The mixture was stirred overnight under N_2 atmosphere. Afterwards, the reacted mixture was adjusted to pH = 2 using hydrochloric acid (1 M), extracted with ethyl acetate (50 mL) and filtered with magnesium sulfate for purification. Subsequently, the product was collected by filtering after precipitation with mineral ether. DMA-MPC copolymer was synthesized by free radical polymerization using AIBN as the initiator. Briefly, DMA and MPC with different mass ratios (total weight: 1 g) were dissolved separately in N, *N*-dimethylformamide (50 mL) under N_2 atmosphere. Afterwards, AIBN (5 mg) was added and the solution was stirred at 68 °C for 24 h. Finally, the mixture was dialyzed against deionized water and freeze dried to obtain the DMA-MPC copolymer.

2.3. Fabrication of copolymer-coated surfaces

All the bare Ti6Al4V sheets were chemically mechanically polished and cleaned by ultrasonication in deionized water for 10 min. The DMA-MPC copolymer solutions (4 mg/mL) were prepared in Tris-HCl buffer (pH = 8.5, 0.5 M). The Ti6Al4V sheets were immersed in the copolymer solutions under ambient condition in the dark for 24 h. For the dopamine assisted codeposition process, the Ti6Al4V sheets were exposed to oxygen plasma for 1 min to remove the potential contaminants and obtain hydroxylated surfaces. A mixture of dopamine (4 mg/mL) and DMA-MPC (4 mg/mL, 1:4) was dissolved in Tris-HCl buffer, and then the Ti6Al4V sheets were coated according to the protocol described above. Afterwards, the Ti6Al4V sheets were rinsed with deionized water and dried under vacuum. The dopamine solution (4 mg/mL) and DMA-MPC copolymer solution (4 mg/mL) were used to modify the Ti6Al4V sheets

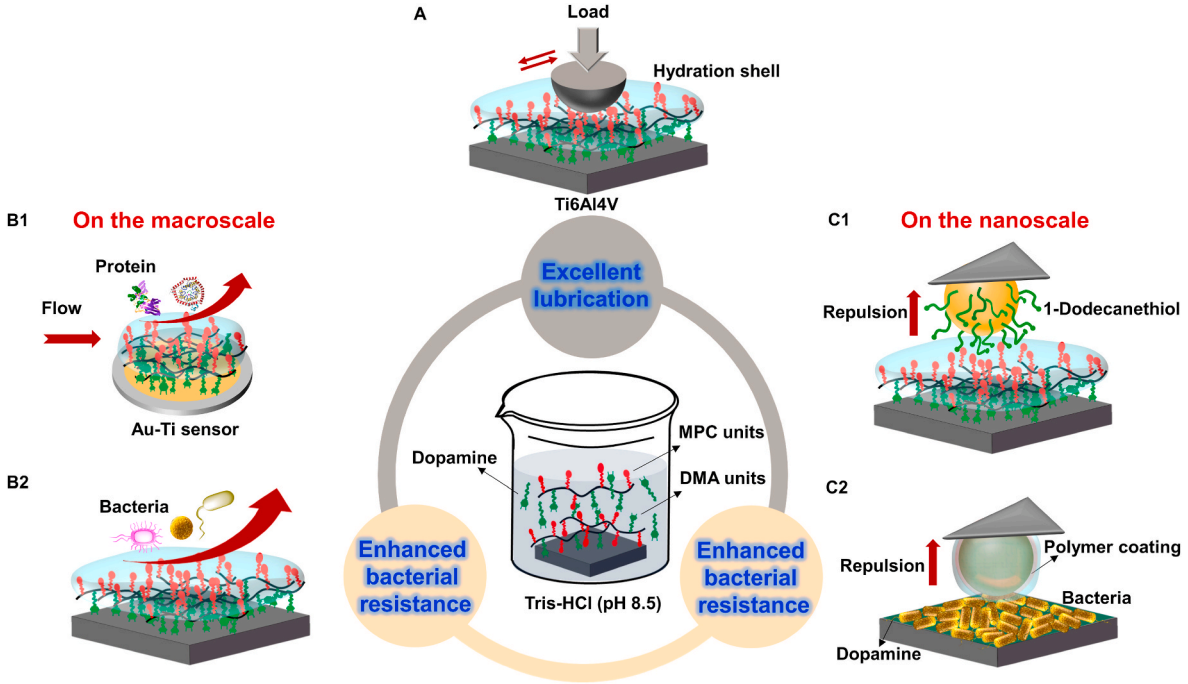

Fig. 1. Illustration showing the facile fabrication of PDA/DMA-MPC biomimetic coating for (A) excellent lubrication property based on hydration lubrication mechanism and (B1–C2) enhanced bacterial resistance property based on hydration repulsion: (B1) quantitative evaluation of dynamic adsorption of proteins on copolymer-coated Au–Ti sensors using QCM, (B2) qualitative/quantitative evaluation of bacterial resistance of copolymer-coated Ti6Al4V substrates, and force measurements probing the interactions between biomimetic coating and (C1) hydrophobic tips or (C2) living bacteria on the nanoscale using AFM.

as controls.

2.4. Characterizations of copolymer-coated surfaces

The ^{1}H nuclear magnetic resonance (NMR) spectra of DMA and DMA-MPC were recorded using a NMR spectrometer (JNM-ECS400, JEOL, Japan), with dimethyl sulfoxide-d6 (DMSO-d_6) and D_2O as the deuterium solvents, respectively. The surface elemental analyses of the Ti6Al4V sheets were evaluated using an X-ray photoelectron spectroscopy (XPS, PHI Quantera II, Ulvac- Phi Inc., Japan) spectrometer with a 15 kV Mg Kα radiation source. The static water contact angles (WCA) were measured by a contact angle goniometer (OCA-20, Dataphysics Instruments, Germany) using a sessile drop method. The surface morphologies of the Ti6Al4V sheets were investigated using an atomic force microscope (AFM, Dimension ICON, Bruker, Germany) under tapping mode with a scan area of 1 μm × 1 μm and a scan rate of 1 Hz. The average surface roughness values of the Ti6Al4V sheets were calculated from at least five measurements.

The adsorption of DMA-MPC or PDA/DMA-MPC on the bare Ti6Al4V sheet was analyzed using a quartz crystal microbalance (QCM, Q Sense Explorer, Biolin Scientific, Sweden). The Au–Ti sensor was prepared via a sputter treatment of the original Au sensor using a sputter meter (JS-3, Institute of microelectronics of the Chinese academy of science, China) to obtain a 15 nm thick titanium film. The Au–Ti sensor was placed into the flow chamber, and then air and Tris-HCl buffer (pH = 8.5, 0.5 M) were pumped over the sensor surface in sequence and stabilized each for 10 min to generate the baseline. Subsequently, DMA-MPC solution (1:4) or a mixture of dopamine and DMA-MPC (1:4) solution in Tris-HCl buffer (concentration: 4 mg/mL) was pumped into the flow chamber for 7 h, which was followed by rinsing of deionized water for 10 min. The flow rate of the solutions used for all the steps was 100 μL/min, and the temperature was 25 °C. The adsorbed mass (Sauerbrey mass) and thickness (Sauerbrey thickness) of the copolymers on the sensors were calculated by the Sauerbrey equation [38] as shown below, where ΔF was the resonant frequency shift of the sensor, and n represented the overtone number (n = 3 in this work, the ordinate of Fig. 3E was processed based on this data).

$$\Delta m = -17.7 * \frac{\Delta F}{n} \left(ng/cm^2\right)$$

$$\Delta \delta = 17.7 * \frac{\Delta F}{100n} \ (nm)$$

In order to evaluate the durability of the copolymer coating, the Ti6Al4V sheets modified with fluorescent copolymer were prepared and fixed in a custom-made rectangular microfluidic channel for flow scouring test, and the stability of the copolymer coating on the substrate was quantitatively monitored by the change of fluorescence intensity at various time intervals. Briefly, the fluorescent copolymer (DMA-MPC-FOM) was synthesized by free radical polymerization similarly to the preparation of DMA-MPC, and the mass of monomers was 0.2 g of DMA, 0.8 g of MPC, and 0.04 g of fluorescein O-methacrylate, respectively. Afterwards, the hydroxylated Ti6Al4V sheets were coated with the DMA-MPC-FOM. The microfluidic device consisted of two parts, including the Ti6Al4V@DMA-MPC-FOM substrate as the lower part and the microfluidic channel as the upper part (height: 100 μm; width: 600 μm), which was made by lithography using polydimethylsiloxane (PDMS, Dow Corning Corp., USA). The punched holes at both ends of the channel were connected with a syringe pump (LSP01-1A, LongerPump, China) by suitable pipes. Phosphate buffer solution (PBS) was used in the flow scouring test with a flow rate of 6 μL/min (the shear stress across the channel was about 4 dyne/cm^2), and the fluorescence intensity at the same location on the Ti6Al4V sheet was monitored by a fluorescence microscope (Ti2–U, Nikon, Japan).

2.5. Tribological tests

The tribological tests were performed using the AFM (MFP-3D-SA, Asylum Research, USA) at room temperature under contact mode. The PS microsphere (diameter: 5 μm) was glued on the jut of the tipless silicon cantilever (TL-CONT, NanoWorld AG, Ne, Switzerland) via curing adhesive, which was irradiated with ultraviolet light for 50 min. The spring constant of the cantilever (K_N: 0.2 N/m) was determined by the frequency calibration method [39], and the lateral sensitivity of the cantilever was obtained by the improved wedge calibration method [40]. The tribological tests were conducted with a normal force of 100–400 nN (corresponding to the contact pressure of 34.4–54.6 MPa), a scan rate of 2 Hz, a sliding distance of 20 μm and a scan area of 20 μm × 20 μm, and the lubricating medium was deionized water. The COF values were calculated from the average of three data points to ensure validity.

2.6. Protein and bacterial resistance of copolymer coating

QCM was used to quantitatively evaluate the dynamic adsorption of bovine serum albumin (BSA) on the copolymer coatings. The Au–Ti sensors were coated with DMA-MPC or PDA/DMA-MPC using the method as described above and placed into the flow chamber. Air and PBS were pumped over the sensor surface in sequence to generate the baseline. Then the BSA solution in PBS (1 mg/mL) was pumped into the chamber at a flow rate of 100 μL/min at 25 °C, which was followed by rinsing of PBS until the measurement was stable.

Escherichia coli (*E. coli*, ATCC8739) was incubated in Luria-Bertani (LB, Sigma-Aldrich, USA) medium overnight, and the bacterial suspension was diluted to a concentration of approximately 1×10^6 CFU/mL. The samples (Ti6Al4V, Ti6Al4V@DMA-MPC and Ti6Al4V@PDA/DMA-MPC in parallel) were sterilized under ultraviolet light for 1 h. Afterwards, the samples were placed in a 24-well plate and incubated with 1 mL of bacterial suspension in an aerobic incubator at 37 °C for 24 h or 8 d (the fresh LB solution was updated daily). For some of the samples incubated for 24 h or 8 d, the bacterial suspensions were removed, and the samples were gently washed with sterile PBS for three times, fixed with 2.5% glutaraldehyde at 4 °C overnight, and sequentially dehydrated using a graded series of ethanol solutions (20%, 40%, 60%, 80% and 100%). Finally, the samples were sputter-coated with platinum and then examined using a scanning electron microscope (SEM, SU8220, Hitachi, Japan) to investigate the bacterial resistance property. For the other samples incubated for 8 d, the biofilm formation on different surfaces was visually observed after being removed from the bacterial suspension. Afterwards, the samples were gently cleaned with sterile PBS for three times and sucked dry with absorbent paper. Then the samples were placed in sterile tubes, and 1 mL of LB solution was added to every tube. The bacteria were dislodged from the surfaces after vortex oscillation for 1 min, and the samples were taken out and washed again with 1 mL of LB solution. The LB solutions were collected, and the bacterial resistance of the copolymer coating was quantitatively characterized by spread plate method. Briefly, 100 μL of bacterial suspension in LB was inoculated onto the triplicate solid agar plates and then incubated at 37 °C overnight. The different colonies were counted, and the bacterial resistance ratio of the copolymer coating was calculated based on the following formula, where $N_{Ti6Al4V}$ represented the bacterial number of the Ti6Al4V group, and N_{Sample} represented the bacterial number of the Ti6Al4V, Ti6Al4V@DMA-MPC, and Ti6Al4V@PDA/DMA-MPC groups, respectively.

$$\text{bacterial resistance ratio } (\%) = \left(N_{Ti6Al4V} - N_{Sample}\right)/N_{Ti6Al4V} \times 100$$

2.7. Force measurements between hydrophilic/hydrophobic AFM tip and copolymer coating

The normal force measurements between hydrophilic/hydrophobic

tip and copolymer coating were performed using AFM in deionized water. The hydrophilic AFM tips were prepared by modifying the PS microspheres with PMPC according to our previous study [14]. Briefly, 0.5 mL of aqueous suspension of amine-modified PS microspheres (25 mg) was mixed with 30 mL of MPC aqueous solution (50 mM), and then 100 μL of TBHP was added as the initiator. The mixture was reacted at 80 °C under N_2 atmosphere for 12 h. Subsequently, the PS microspheres were collected by centrifugation, dried under vacuum, and glued on the jut of the tipless silicon cantilever using the method as described above. For the preparation of hydrophobic AFM tips, the PS microspheres were sputter-coated with a 10 nm thick platinum layer, and immersed in 1-dodecanethiol solution in ethanol (1 mmol/L) for 24 h to form a self-assembled methyl group-terminated surface, followed by drying under vacuum. The surface morphologies and elemental compositions of the AFM tips were examined by SEM associated with an energy dispersive spectrometer (EDS). To confirm the successful preparation of the hydrophobic AFM tips, the same procedure was used to modify the PS plate, and the WCA values of platinum treated PS plate (PS@Pt) and 1-dodecanethiol treated PS@Pt were measured for comparison.

The spring constant of the hydrophilic/hydrophobic AFM tips was in the range of 0.10–0.25 N/m. Before the normal force measurements, the AFM tips against different substrates (including bare Ti6Al4V, Ti6Al4V@DMA-MPC and Ti6Al4V@PDA/DMA-MPC) were immersed in deionized water for 10 min to allow for the stretching of the polymer chains. During the force measurement, the tip was driven to approach and touch the substrate at a velocity of 1 μm/s until the maximum contact force reached 10 nN, and then it was retracted immediately from the substrate at the same velocity. A force-distance curve was recorded automatically in the approach and separation process. The adhesion force was determined by the absolute value of the difference between the baseline and the lowest point in the separation curve, and the adhesion energy was calculated by the regional integration of the separation curve below the baseline. The force measurements were conducted for at least 30 various locations on the substrate, and at least two independent AFM tips were tested to ensure validity.

2.8. Force measurements between copolymer-coated AFM tip and bacteria

To measure the interactions between copolymer coating and bacteria on the nanoscale, two contact surfaces were prepared, including an immobilized bacteria (*E. coli*) coated Ti6Al4V substrate and a DMA-MPC or PDA/DMA-MPC coated AFM tip. The PS microspheres were sputter-treated with a titanium film (thickness: 15 nm), coated with DMA-MPC or PDA/DMA-MPC for 24 h using the method as described above, and finally dried under N_2 atmosphere. The AFM tips were sterilized under ultraviolet light for 1 h before the force measurements. The bacteria-coated substrates were prepared with the assistance of dopamine as a wet bio-adhesive. Briefly, the Ti6Al4V sheets were immersed in dopamine solution (4 mg/mL, dissolved in Tris-HCl buffer) in the dark for 10 h. Next, the substrates were washed with sterile PBS, dried under N_2 atmosphere, and placed in the 24-well plate for sterilization under ultraviolet light for 1 h. Afterwards, the substrates were incubated with 1 mL of *E.coli* suspension (1×10^8 CFU/mL) at 37 °C for 48 h in the aerobic incubator, and fresh LB medium was added to the suspension per 12 h. The bacterial coverage on the substrates was examined using a digital microscope (VHX-100, Keyence, Japan) to ensure sufficient density. The bacterial suspensions were removed, and the substrates were gently washed with 0.85% NaCl for three times. Meanwhile, the activity of bacteria was checked using a Live/Dead Baclight bacterial viability kit (L7012, Thermo Fisher Scientific, USA). Briefly, equal volumes of SYTO 9 (1.5 μL, green fluorescent nucleic acid stain) and propidium iodide (1.5 μL, red fluorescent nuclear and chromatin counterstain) were combined in a microfuge tube and dissolved in deionized water (1 mL) in the dark. The dye mixture (200 μL) was added dropwise to the surface of the substrate and incubated at room temperature for 15 min in the dark. The excrescent dye was removed, and the substrates were gently washed with 0.85% NaCl for three times. Afterwards, the bacterial viability was checked using a laser scanning confocal microscope (LSM710, ZEISS, Germany) before the force measurements.

The calibration of copolymer-coated AFM tips was performed using the same method as described above, and the spring constant of the tips in sterile PBS was in the range of 0.10–0.25 N/m. The force measurements were conducted in sterile PBS, during which the tip was driven to approach the substrate at a velocity of 1 μm/s until the maximum contact force reached 2 nN. The AFM tip contacted with the substrate with different dwell times of 0, 10 and 30 s and then retracted from the substrate at the same velocity. The adhesion force and adhesion energy were calculated based on the methods as described above. Each force measurement was repeated on at least 10 different locations on the substrate, and at least three independent tips were tested. The force-distance curves of bare and DMA-MPC coated AFM tips were used as controls. The bacterial viability was further checked following the force measurements to ensure the validity of the tests.

3. Results and discussion

3.1. Design and synthesis of self-adhesive lubricated coating

The self-adhesive copolymer DMA-MPC consisted of a synthetic self-anchoring agent DMA and a lubrication unit MPC. The DMA and DMA-MPC were synthesized according to our previous protocols [27–29], with the detailed information provided in Supporting Information. In order to obtain copolymers with diverse contents of lubricated groups for screening, three different proportions of copolymers were prepared to examine lubrication property. Therefore, DMA-MPC with the mass ratio of 1:4, 1:1 and 4:1 (DMA/MPC) was applied to modify the titanium alloy (Ti6Al4V) substrate, namely Ti6Al4V@DMA-MPC. Fig. 2A shows the ^{1}H NMR spectrum of the three kinds of DMA-MPC. The ^{1}H NMR spectrum of DMA is provided in Fig. S1. The signals at 7.87 and 6.87 ppm are assigned to DMA, and the signal at 3.16 ppm corresponds to the characteristic groups of MPC. The XPS presents the elemental compositions of the samples. As shown in Fig. 2B, compared with bare Ti6Al4V, the presence of N 1s (402.0 eV) and P 2p (133.3 eV) peaks for Ti6Al4V@DMA-MPC confirms the successful modification of DMA-MPC on Ti6Al4V. In addition, the WCA also prove the modification process, which are greatly decreased from 78.6° for Ti6Al4V to 35.2°, 40.8° and 52.8° for the three kinds of Ti6Al4V@DMA-MPC, respectively (Fig. 2C). Generally, the enhanced hydrophilicity is attributed to the phosphorylcholine groups in MPC, in which the zwitterionic charges ($-PO_4^-$ and $-N^+(CH_3)_3$) have excellent hydration property.

A series of tribological tests were performed using AFM in contact mode to investigate the lubrication property of the DMA-MPC copolymers. Fig. 2D displays the schematic illustration of the tribological measurement, using a typical contact friction pair setup with PS microsphere and different Ti6Al4V substrates. Fig. 2E shows the COF values under four normal force conditions, and the corresponding maximum contact pressures are 34.4 (100 nN), 43.4 (200 nN), 49.6 (300 nN) and 54.6 MPa (400 nN), respectively. The COF values for the three proportions of Ti6Al4V@DMA-MPC are all lower than that of Ti6Al4V, which is in good agreement with our previous study [29]. Generally, the Ti6Al4V@DMA-MPC at the mass ratio of 1:4 results in the most significant reduction in the COF value, which decreases dramatically from 0.136 to 0.025 (81.3%, 34.4 MPa). Additionally, there is no obvious difference for the Ti6Al4V@DMA-MPC at the mass ratio of 1:4 and 1:1. The enhanced lubrication is attributed to the hydration lubrication mechanism of the phosphorylcholine groups as described above [10]. Overall, the tribological test indicates that the DMA-MPC at the mass ratio of 1:4 produces optimal lubrication enhancement, and thus the following experiments are performed using this copolymer.

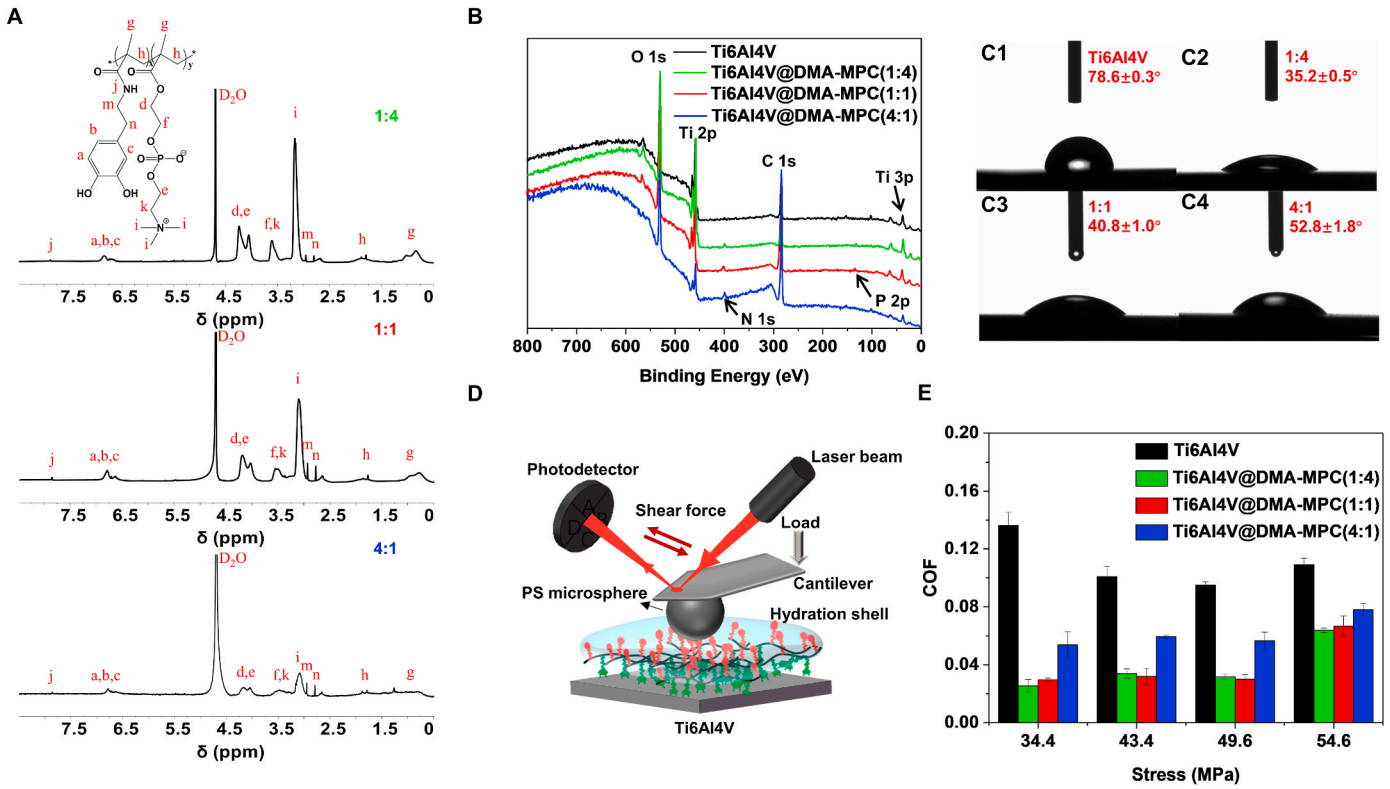

Fig. 2. Material characterizations and tribological measurements. (A) ^{1}H NMR spectra of three different proportions of copolymers DMA-MPC. (B) XPS and (C1–C4) WCA of bare Ti6Al4V and three kinds of Ti6Al4V@DMA-MPC. (D) Schematic illustration showing the setup of tribological measurements, with a typical contact pair between PS microsphere and Ti6Al4V substrate. (E) The COF values under four normal force conditions in the tribological measurements.

3.2. Dopamine-assisted codeposition of lubricated coating for bacterial resistance

To obtain a stable self-adhesive lubricated coating for bacterial resistance, a dopamine-assisted codeposition technique was applied to optimize surface modification of the copolymer DMA-MPC on the Ti6Al4V substrate. The Ti6Al4V substrate was previously treated with plasma to generate hydroxylated surface, which could effectively strengthen the coordination (or chelating) bonding between the catechol groups (in dopamine and DMA) and the substrate. Subsequently, a series of surface modifications on the Ti6Al4V substrate were conducted for further evaluation, including Ti6Al4V@PDA, Ti6Al4V@DMA-MPC and Ti6Al4V@PDA/DMA-MPC.

The elemental compositions of the samples characterized by XPS are shown in Fig. 3A. The presence of the P 2p (133.3 eV) peak in Ti6Al4V@DMA-MPC and Ti6Al4V@PDA/DMA-MPC confirms the successful modification of the copolymers on the substrate. It is also proved by the high-resolution narrow spectrum of P 2p in Fig. S2A, where a typical peak is observed for both Ti6Al4V@DMA-MPC and Ti6Al4V@PDA/DMA-MPC. Additionally, the characteristic peak of N 1s (402.0 eV) for Ti6Al4V@PDA indicates the successful modification of PDA on the substrate. The high-resolution narrow spectra of N 1s are deconvoluted into five types, which correspond to the amide and quaternary ammonium groups (−NHCO−, $-N^{+}(CH_3)_3$) in DMA-MPC and other there related amine complexes (R–NH_2, R–NH_3^{+}, RC = N−) within PDA, respectively (Fig. 3B). The reduced ratio of Ti 2p/N 1s further indicates that the copolymer DMA-MPC has been successfully modified on the Ti6Al4V substrate.

The WCA of hydroxylated Ti6Al4V is significantly higher than that of the samples following surface modification (Fig. 3C), which further verifies the successful coating process. Actually, hydrophilicity is associated with the polar groups (e.g. phosphorylcholine group) and the surface roughness. The surface morphologies of the samples characterized by AFM are shown in Fig. 3D. Ti6Al4V@PDA has a relatively higher surface roughness (*Ra*: 14.5 nm) and leads to a better surface wettability (WCA: 26.1°), compared with hydroxylated Ti6Al4V (WCA: 52.5°) under the condition of wetting. The increased surface roughness of the PDA coating is mainly ascribed to the agglomeration stacking and inhomogeneous deposition between the PDA molecules [41,42]. As indicated in previous studies [43,44], PDA coating can assemble via the interactions of covalent bond and noncovalent bond between various heterogeneous derivatives. Specifically, the noncovalent self-assembly process involves intermolecular interactions such as hydrogen bond, π−π stacking, cation−π interaction and van der Waals interaction. The incorporation of DMA-MPC results in a relatively smooth and uniform PDA/DMA-MPC coating on the Ti6Al4V substrate, and the surface roughness greatly reduces to 1.7 nm. Generally, dopamine-assisted codeposition with DMA-MPC can decrease the agglomeration stacking and inhomogeneous deposition of PDA, and facilitate the progressive assembly of multi-layered DMA-MPC coating. It has been indicated that the cation−π interaction is the primary mechanism for intermolecular assembly in the construction of dopamine-related coating [45], and the strong interaction exists not only within PDA molecules but also between DMA-MPC and PDA. In addition, the interaction between aromatic rings in PDA and zwitterionic charges of phosphorylcholine in MPC segment, such as phenol-phospholipid hydrogen bond and cation−π interaction between the quaternary ammonium groups and aromatic rings, also mediates the compound deposition. Consequently, PDA, as an intercalated agent, can effectively facilitate the self-adhesive coating process.

To further characterize the self-adhesion and self-assembly behavior of the biomimetic coating, QCM with dissipation monitoring was employed to quantitatively evaluate the copolymer adsorption performance. The frequency change (ΔF) of the sputter-treated QCM sensor (Au–Ti) reflects the change in the adsorbed mass (Sauerbrey mass) [38]. The resulting ΔF obtained for the DMA-MPC and PDA/DMA-MPC

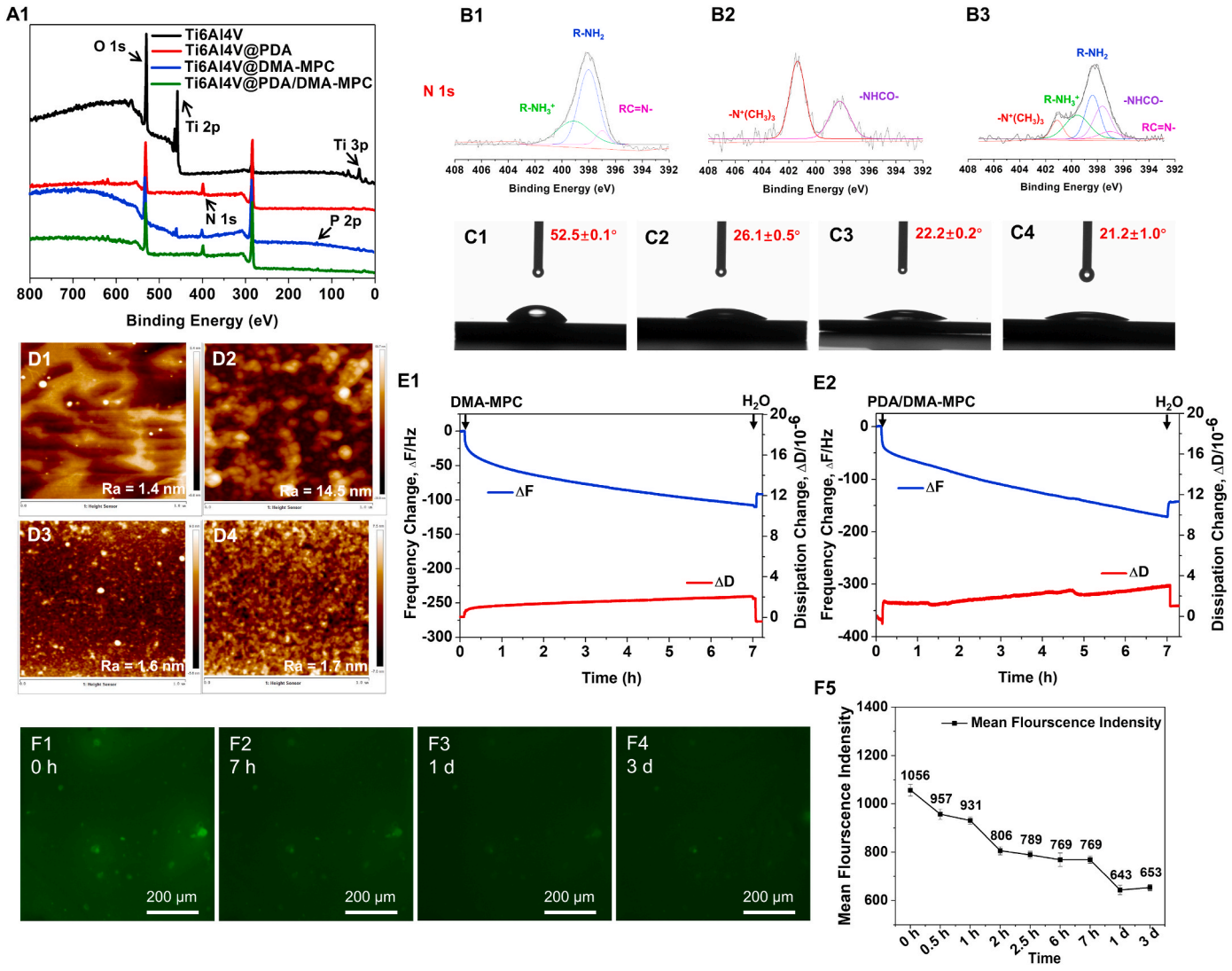

Fig. 3. (A) XPS of four different Ti6Al4V substrates. (B) High-resolution narrow spectrum of N 1s for (B1) Ti6Al4V@PDA, (B2) Ti6Al4V@DMA-MPC and (B3) Ti6Al4V@PDA/DMA-MPC. (C) WCA and (D) surface morphologies of (C1, D1) Ti6Al4V, (C2, D2) Ti6Al4V@PDA, (C3, D3) Ti6Al4V@DMA-MPC (1:4) and (C4, D4) Ti6Al4V@PDA/DMA-MPC (1:4). The Ti6Al4V substrates were treated with plasma to obtain hydroxylated surfaces. (E) Frequency and dissipation changes associated with the self-adhesive biomimetic coating for (E1) DMA-MPC and (E2) PDA/DMA-MPC. (F) Quantitative characterization of the durability of the copolymer coating by monitoring the change of fluorescence intensity in the microfluidic channel under flow scouring test. The fluorescence images of various scouring times: (F1) 0 h, (F2) 7 h, (F3) 1 d, and (F4) 3 d (F5) The change of fluorescence intensity at different scouring times.

coating during exposure to a corresponding copolymer solution followed by H_2O rinsing is shown in Fig. 3E. The Sauerbrey mass of the DMA-MPC and PDA/DMA-MPC coating on the Au–Ti sensor is 1616.1 and 2492.2 ng/cm^2 within 7 h, and the Sauerbrey thickness is 16.2 nm and 24.9 nm. Moreover, the relatively inconspicuous change of dissipation (ΔD) indicates slight viscoelasticity of the biomimetic coating. Consequently, it is considered that the as-fabricated coating can be roughly regarded as a rigid membrane. In addition, the dry thickness of the DMA-MPC and PDA/DMA-MPC coatings on Ti6Al4V substrate for 24 h is approximately 20 nm and 33 nm, which is tested by ion beaming stripping technology using XPS. Overall, the above data indicate that dopamine-assisted codeposition generates a much thicker and relatively soft coating compared with the copolymer coating. Furthermore, the great reduction in WCA of the Au–Ti sensors after QCM measurement (Fig. S2B) further confirms the adsorption of the copolymers on the substrates.

The durability of the copolymer coating was quantitatively characterized by monitoring the change of fluorescence intensity in the microfluidic channel under flow scouring test. As shown in Fig. 3F1-F4, the fluorescence intensity of Ti6Al4V@DMA-MPC-FOM gradually decreases as the scouring time increases, especially with a faster reduction at day 1, which is attributed to the shedding of the weakly adsorbed copolymers. However, as can be seen from Fig. 3F5, the fluorescence intensity basically reaches stable at day 3, which proves that the copolymer coating has good durability and stability.

Similar to the results of above tribological test, the PDA/DMA-MPC coating also has excellent lubrication property. As shown in Fig. S3A, the COF of Ti6Al4V@PDA is just slightly decreased compared with the hydroxylated Ti6Al4V, which is probably owing to the relatively rough surface. However, Ti6Al4V@DMA-MPC and Ti6Al4V@PDA/DMA-MPC still maintain low COF values, and there is no significant difference between these samples. The slight increase in the COF value for Ti6Al4V@PDA/DMA-MPC, compared with that of Ti6Al4V@DMA-MPC, can be attributed to the incorporation of PDA, where a higher surface roughness and the local surface inhomogeneity may affect the lubrication performance. Moreover, it is noted that the lubrication property of the PDA/DMA-MPC coating is stable under different contact pressures.

Bacterial adhesion is generally divided into three stages, which begins with a reversible initial adhesion. It is followed by the transition to an enhanced irreversible adhesion and finally develops into a mature biofilm [15]. Therefore, inhibiting initial bacterial adhesion is the key to prevent biofilm formation. Previous studies have indicated that many bacterial cells contain various proteinaceous extracellular appendages that have direct or indirect roles in adhesion [21], such as the flagellum, pili, curli and so on [17–20]. Consequently, protein and bacterial resistance of the biomimetic coating were firstly investigated on the macroscale. QCM was applied to quantitatively evaluate the dynamic adsorption of the representative protein (BSA) on the bare and copolymer-coated Au–Ti sensors. The bare and DMA-MPC coated Au–Ti sensors were used as control. It is clearly shown from Fig. 4A that the PDA/DMA-MPC coating has superior anti-protein adhesion property, in which the Sauerbrey mass of BSA adsorption (60.2 ng/cm^2) is significantly lower than that of either the bare (1185.9 ng/cm^2) or DMA-MPC coated (219.5 ng/cm^2) sensors. Similarly, the results of bacterial resistance experiments examined using spread plate method and SEM are consistent with the QCM measurement, as shown in Fig. 4B and C and Fig. S3B. The samples were carried out by spread plate assay after culturing for 8 days. Fig. 4B1 shows the bacterial resistance ratio and Fig. 4B2-B4 illustrates the colony images of different substrates. It is clear that the bacterial resistance ratio of Ti6Al4V@DMA-MPC and Ti6Al4V@PDA/DMA-MPC is larger than 80%. Interestingly, the bacterial resistance ratio of Ti6Al4V@PDA/DMA-MPC is as high as 98%, indicating that the copolymer coating has excellent hydration repulsion for bacterial resistance.

After the bacteria contact with a surface, the initial 24 h is considered to be the "decisive period" to prevent bacterial adhesion. Therefore, the bacterial resistance property of the samples (bare or copolymer-coated Ti6Al4V) is discussed by incubation in *E. coli* suspension for 24 h. Clearly, the bare Ti6Al4V substrate (Fig. 4C1) suffers from severe bacterial adhesion, whereas only very few adherent bacteria are observed on the surface of Ti6Al4V@DMA-MPC (Fig. 4C2) or Ti6Al4V@PDA/DMA-MPC (Fig. 4C3). Similarly, after incubation in *E. coli* suspension for 8 d, the representative SEM images shows very small amount of bacteria adhesion on the surface of Ti6Al4V@DMA-MPC (Figure S3B2) and even less for Ti6Al4V@PDA/DMA-MPC (Figure S3B3), compared with that of bare Ti6Al4V substrate (Figure S3B1). Meanwhile, the biofilm formation of Ti6Al4V@PDA/DMA-MPC is significantly weaker than that of bare Ti6Al4V and Ti6Al4V@DMA-MPC. These results are attributed to the tenacious hydration layer formed around the zwitterionic charges of the phosphorylcholine groups in MPC, which can generate a strong repulsive force on the bacteria when they approach the surface for adhesion [29]. Additionally, Tanaka et al. have also proposed the "intermediate water concept" for the interpretation of water-mediated repulsive force, in which the physical barrier of the intermediate water plays an important role in preventing protein

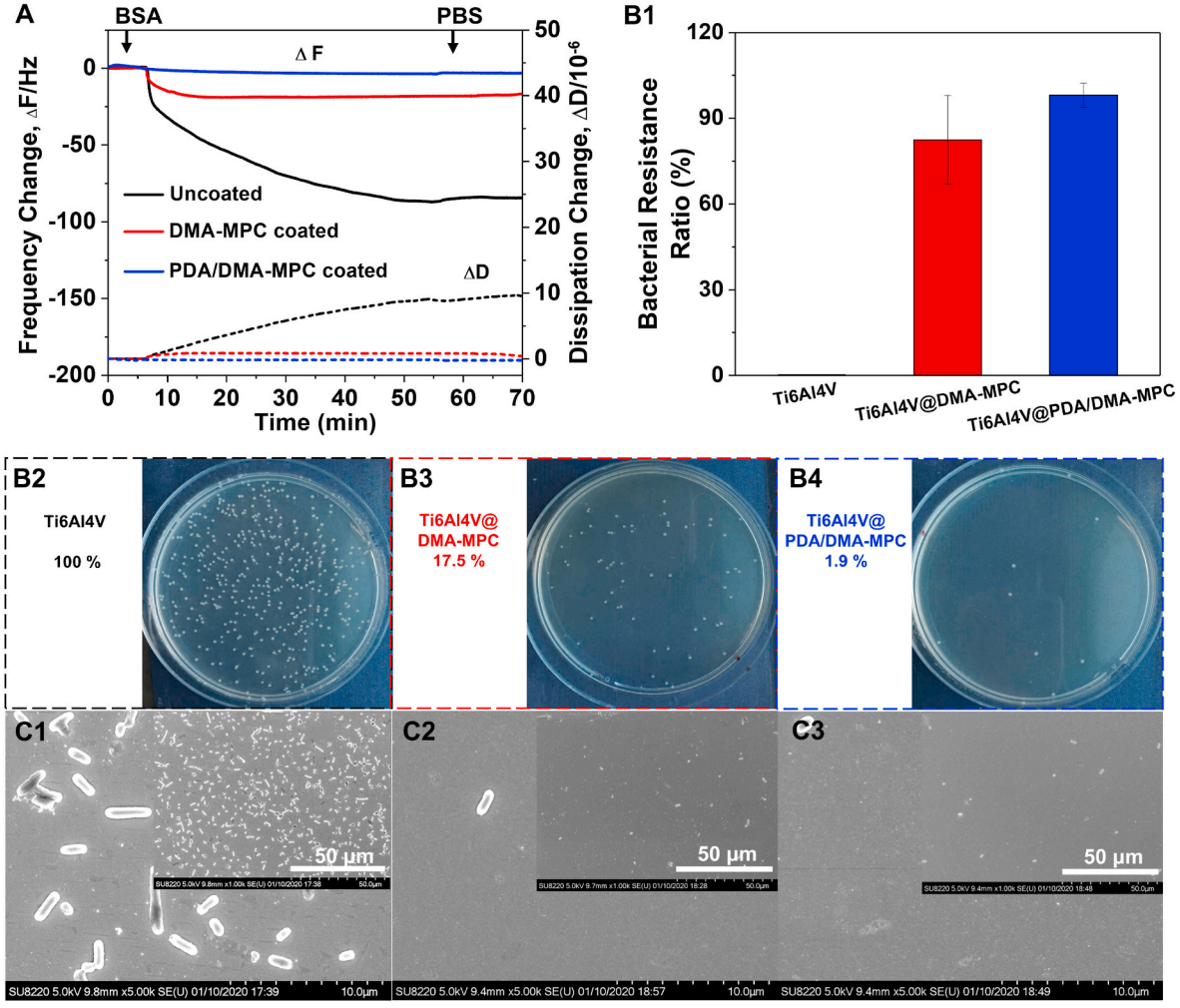

Fig. 4. (A) Frequency and dissipation changes associated with dynamic adsorption of BSA on bare and copolymer-coated Au–Ti sensors. (B) The bacterial resistance property tested by spread plate assay. (B1) The bacterial resistance ratio of different substrates. The colony images of (B2) bare Ti6Al4V, (B3) Ti6Al4V@DMA-MPC, and (B4) Ti6Al4V@PDA/DMA-MPC with the bacterial count as 100%, 17.5%, and 1.9%, respectively. (C) Representative SEM images showing *E. coli* adhesion on the Ti6Al4V substrates after culturing for 24 h: (C1) bare Ti6Al4V, (C2) Ti6Al4V@DMA-MPC, and (C3) Ti6Al4V@PDA/DMA-MPC.

adsorption on the substrate [46]. Overall, the QCM, spread plate assay, and SEM results indicate that the dopamine-assisted PDA/DMA-MPC coating effectively enhances anti-protein and bacterial resistance on the macroscale.

3.3. Interactions between copolymer coating and hydrophilic/hydrophobic AFM tips

To probe the potential interactions between the biomimetic coating and bacteria on the nanoscale, a series of force measurements were first performed to examine adhesion between the copolymer coating and hydrophilic/hydrophobic AFM tips under aqueous conditions. The hydrophilic AFM tips were prepared by coating PMPC on the surface of the PS microspheres, and the hydrophobic AFM tips were fabricated by coating the PS microspheres with the self-assembled 1-dodecanethiol layer, which was used to mimic the hydrophobic domains within the proteins and proteinaceous extracellular appendages in bacteria. The SEM and EDS results of different AFM tips are displayed in Fig. S4. The comparison of WCA between the Pt-treated PS plate (PS@Pt) and PS@Pt following self-assembly of the 1-dodecanethiol layer (Fig. S5A) supports the successful preparation of the hydrophobic AFM tips.

Fig. 5 shows the representative force-distance curves in the force measurements during the approach and separation process of the hydrophilic (Fig. 5A) and hydrophobic AFM tips (Fig. 5B) against the substrates of bare Ti6Al4V, Ti6Al4V@DMA-MPC and Ti6Al4V@PDA/DMA-MPC. All the measurements indicate the short-range steric repulsion force in the approach process from the hard-wall repulsion. Notably, the hydrophobic AFM tips show longer range of repulsion, compared with the hydrophilic AFM tips. It is considered that the gradual increase from the bare Ti6Al4V to Ti6Al4V@PDA/DMA-MPC is due to the mutually exclusive hydrophobic interactions, which indicates that the PDA/DMA-MPC coating can act as an energy barrier to prevent or delay the adsorption of protein or bacteria. However, in the case of the hydrophilic AFM tips, there are strong attractive forces toward the two hydrophilic surfaces due to the capillary force [47], which are produced by the hydrated meniscus of the MPC domains within the opposing two surfaces (Fig. 5A2, A3). The attractive forces present in a relatively long range (larger than 1000 nm) are initially caused by the fusion of water molecules from the topmost hydration layers, which are generated by the charge-dipole interactions between zwitterionic charges and water molecules. The attractive force for bare Ti6Al4V is weaker in the approach process. However, there is an obvious jump-in at the distance of 60 nm and after that the attractive force starts to appear (Fig. 5A1). This is attributed to the capillary force that is caused by the fusion of the hydration layer in PMPC and the hydrated hydroxylated Ti6Al4V surface.

Regarding the separation process, a short-range (extending for a distance of approximately 150 nm) adhesion force is observed between the bare Ti6Al4V and hydrophilic AFM tips (Fig. 5A1), indicating the presence of capillary force and also electrostatic, van der Waals and hydrogen bond forces. Note that the latter three interactions exist in all force measurements. The repulsion between the bare Ti6Al4V and hydrophobic AFM tips is almost completely reversible with no hysteresis (Fig. 5B1), which indicates that no adhesion forces can be detected in this case. On the contrary, a typical pattern of oscillatory adhesion forces is observed for the hydrophilic AFM tips against Ti6Al4V@DMA-MPC and Ti6Al4V@PDA/DMA-MPC (Fig. 5A2, A3). This is attributed to the penetration of the hydrophilic AFM tips into the DMA-MPC domains of the substrates, resulting in unraveling and stretching of the polymer chains in the separation process [33]. The largest adhesion force between the hydrophilic AFM tips and Ti6Al4V@PDA/DMA-MPC reflects the extra energy of stretching between PDA and DMA-MPC (Fig. 5A4). Additionally, the increased extension distance of the adhesion force for Ti6Al4V@PDA/DMA-MPC (~1000 nm), compared with that of Ti6Al4V@DMA-MPC (~800 nm), may be ascribed to the rearrangement of the PDA and DMA-MPC chains. Since DMA-MPC is not covalently bound to PDA, the polymer chains can rearrange to form a more optimal conformation during the separation process [5]. As shown in Fig. 5B2, B3, a different pattern of oscillatory adhesion forces is produced for the hydrophobic AFM tips against Ti6Al4V@DMA-MPC and Ti6Al4V@PDA/DMA-MPC, with decreased extension distances and reduced values of adhesion forces (Fig. 5B4). The hysteresis is owing to the mutually attractive hydrophobic interactions [33,47,48] between the methyl groups in the end-domains of 1-dodecanethiol and aromatic groups or methyl residues in the polymer chains. It is anticipated that although the asymmetric configurations between the polymer and 1-dodecanethiol can hinder penetration [34], the hydrophobic AFM tips still penetrate into the copolymer coatings to some extent. Furthermore, the adhesion forces and adhesion energies obtained from the separation process (Fig. 5A4, B4) show clearly that the hydrophobic AFM tips generate smaller values in comparison with the hydrophilic AFM tips when interacting with the copolymer coatings. The increased values of adhesion forces and adhesion energies for the substrates with copolymer coatings, compared with the bare Ti6Al4V, are attributed to the use of a relatively high normal load (10 nN), resulting in the penetration of the AFM tips into the copolymer coatings. In summary, the strongest repulsion with the longest range of the hydrophobic AFM tips in the approach process indicates that the PDA/DMA-MPC coating plays a significant role in preventing or delaying initial adsorption of protein or bacteria. Therefore, further research is performed to investigate the interactions between the copolymer coatings and living bacteria.

3.4. Repulsive force between copolymers-coated AFM tips and bacteria on the nanoscale

To further evaluate the initial bacterial resistance properties of the copolymer coatings on the nanoscale, a series of force measurements were conducted to investigate the interactions between the copolymer coatings and living bacteria in sterile PBS using AFM. The two contact surfaces included a copolymers-coated AFM tip and an immobilized bacteria (*E. coli*)-coated Ti6Al4V substrate. The AFM tips (with PS microspheres) were sputter-treated with a titanium layer and coated with the copolymers according to the protocol of modifying the Ti6Al4V substrates. The bacteria-coated Ti6Al4V substrates were prepared using a poly-dopamine wet bio-adhesive [49,50], which could effectively immobilize bacteria on the substrate and meanwhile ensure the viability of the bacteria during the force measurements.

The SEM and EDS results of the copolymers-coated AFM tips are shown in Fig. S4, which indicate that the coating process is successful. Fig. 5C1 displays the schematic illustration of the force measurements, in which the copolymers-coated AFM tip is driven to gradually approach and touch the bacterial Ti6Al4V substrate at a maximum contact force of 2 nN. Subsequently, it is retracted from the substrate at the same velocity with different dwell times of 0 s, 10 s and 30 s. It is noted that due to the geometry limitation of the PS microspheres, only a few bacteria are allowed to contact with the AFM tips. However, the microscopy image of the substrate (Fig. 5C2) shows that the substrate has reached a sufficiently dense coverage of bacteria, which ensures the validity of the measurements on randomly selected locations for statistical analysis. Fig. 5C3 illustrates representative microscopy image during the force measurements between the copolymers-coated AFM tip and the bacteria-coated substrate, and the comparison of the microscopy images for the substrates with or without bacteria are shown in Fig. S5B. Importantly, the bacteria immobilized on the substrate maintain excellent viability, as observed from the Live/Dead fluorescence staining images before (Fig. 5C4) and after (Fig. 5C5) the force measurements. More importantly, no obvious fluorescence is detected on the AFM tips following the force measurements, indicating the robustness of the test as the bacteria are not removed from the substrate under the experimental conditions.

Fig. 5D1-D3 shows representative force-distance curves in the force measurements of the bare titanium-coated tip (Ti tip), DMA-MPC-coated

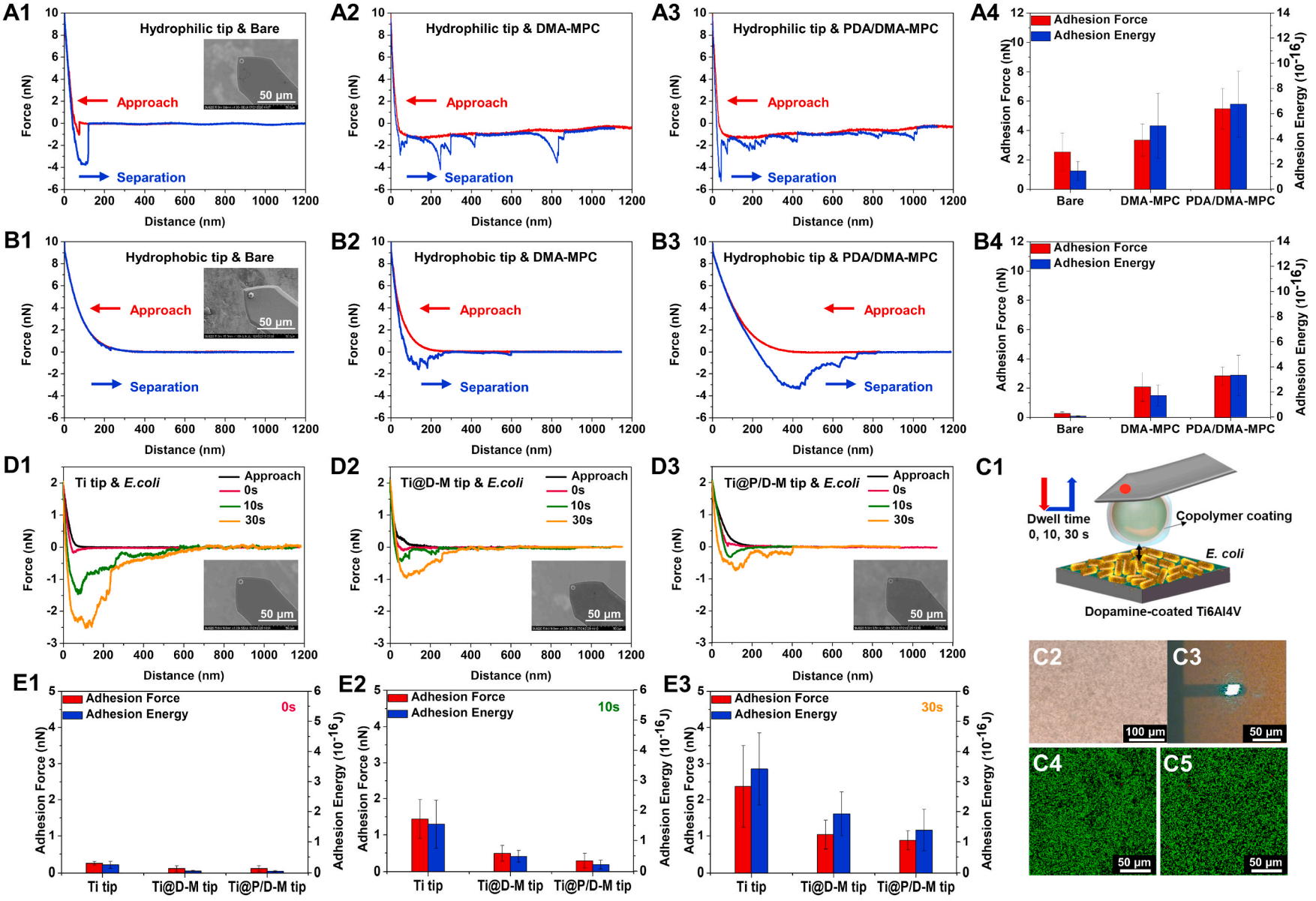

Fig. 5. Representative force-distance curves during approach and separation process in the force measurements using AFM for (A1-A3) hydrophilic tip and (B1–B3) hydrophobic tip against the bare Ti6Al4V, Ti6Al4V@DMA-MPC and Ti6Al4V@PDA/DMA-MPC substrates. The inset figures are the SEM images of the tips. (A4, B4) Statistical analysis of adhesion force and adhesion energy obtained from the separation process. (C1) Schematic illustration showing the force measurements between copolymer-coated AFM tip against bacteria-coated substrate, with different dwell times of 0 s, 10 s and 30 s (C2) Microscopy images of the bacteria-coated substrate. (C3) Microscopy images in the force measurements between AFM tip and bacteria-coated substrate. The green fluorescence indicates that the immobilized bacteria are alive (C4) before and (C5) after the force measurements. (D) Representative force-distance curves during approach and separation process in the force measurements for (D1) Ti tip, (D2) Ti@D-M tip and (D3) Ti@P/D-M tip against bacteria-coated substrates. (E) The adhesion force and adhesion energy between three different AFM tips and bacteria-coated substrates obtained from the separation process under the dwell time of (E1) 0 s, (E2) 10 s and (E3) 30 s. (For interpretation of the references to colour in this figure legend, the reader is referred to the Web version of this article.)

Ti tip (Ti@D-M tip) and PDA/DMA-MPC-coated Ti tip (Ti@P/D-M tip) against the bacterial Ti6Al4V substrates under different dwell times, respectively. Again, all the force measurements show the hard-wall steric repulsion in the approach process. Compared with the Ti tip, the Ti@D-M tip and Ti@P/D-M tip indicate gradually increased range of repulsion force due to the mutually exclusive hydrophobic interactions. These results are similar to the findings as shown in Fig. 5B, which indicate that the strong energy barrier of the PDA/DMA-MPC copolymer has the best bacterial resistance effect owing to the stable hydration repulsion layer. In the separation process, it is clear that the adhesion force and adhesion interaction range are observed to increase at higher surface dwell time for the three kinds of AFM tips. It is considered that the longer dwell time allows for the bacteria to adapt to the topography of the contact surface more effectively. This results in an increased contact area that may generate more specific interactions between the AFM tips and bacteria, such as electrostatic, van der Waals and hydrogen bond forces. Interestingly, the adhesion force or adhesion interaction range of the Ti@P/D-M tip is lower or shorter than the Ti@D-M tip and Ti tip under all experimental conditions, which indicates that the Ti@P/D-M tip can provide a relatively larger hydration repulsion to resist bacterial adhesion. The statistical histograms (Fig. 5E1-E3) of the adhesion force and adhesion energy intuitively display the comparison among the three AFM tips against bacteria under various dwell times. For example, the adhesion force between Ti@P/D-M tip and bacteria is approximately 0.88 nN under the dwell time of 30 s, which is smaller than that of Ti@D-M tip (1.04 nN) and Ti tip (2.37 nN). Similarly, the adhesion energy between Ti@P/D-M tip and bacteria is also the lowest (1.39E-16 J), compared with that of Ti@D-M tip (1.93E-16 J) and Ti tip (3.42E-16 J). In summary, the Ti@P/D-M tip generates the strongest and longest range of repulsion in the approach process and also the lowest adhesion force and shortest adhesion interaction range in the separation process. These results reveal that the biomimetic PDA/DMA-MPC coating greatly enhances the bacterial resistance performance.

4. Conclusions

In the present study, motivated by the performance of mussel and articular cartilage, a bioinspired self-adhesive lubricated copolymer coating was developed for the purpose of enhancing bacterial resistance. The dopamine-assisted codeposition technique was used to fabricate optimal biomimetic PDA/DMA-MPC coating on the substrate to simultaneously achieve lubrication and bacterial resistance properties. Additionally, the mechanism of bacterial resistance was reported by investigating the interactions between the biomimetic coatings and hydrophilic/hydrophobic tips or living bacteria on the nanoscale via AFM force measurements. The results showed that the biomimetic copolymer coating performed excellent lubrication property based on the hydration lubrication mechanism, and effectively enhanced bacterial resistance both on the macroscale and nanoscale owing to hydration repulsion. In conclusion, the self-adhesive lubricated copolymer coating developed here can be a promising strategy in surface functionalization of biomedical implants for enhancing bacterial resistance.

CRediT authorship contribution statement

Ying Han: Investigation, Methodology, Writing - original draft. **Weiwei Zhao:** Methodology, Formal analysis, Writing - review & editing. **Yiwei Zheng:** Methodology. **Haimang Wang:** Formal analysis. **Yulong Sun:** Formal analysis. **Yifei Zhang:** Resources. **Jing Luo:** Visualization. **Hongyu Zhang:** Conceptualization, Resources, Writing - review & editing, Funding acquisition.

Declaration of competing interest

The authors declare no conflict of interest.

Acknowledgements

This study was financially supported by National Natural Science Foundation of China (52022043), Tsinghua University Initiative Scientific Research Program (20197050026), Precision Medicine Foundation, Tsinghua University, China (10001020120), Capital's Funds for Health Improvement and Research (2020-2Z-40810), and Research Fund of State Key Laboratory of Tribology, Tsinghua University, China (SKLT2020C11).

Appendix A. Supplementary data

Supplementary data to this article can be found online at https://doi.org/10.1016/j.bioactmat.2021.01.028.

References

[1] T. Røn, K.P. Jacobsen, S.H. Lee, A catheter friction tester using balance sensor: combined evaluation of the effects of mechanical properties of tubing materials and surface coating,, J. Mech. Behav. Biomed. Mater 84 (2018) 12–21.
[2] Y.Y. Jiao, S.Z. Liu, Y.L. Sun, W. Yue, H.Y. Zhang, Bioinspired surface functionalization of nanodiamonds for enhanced lubrication, Langmuir 34 (2018) 12436–12444.
[3] M. Kyomoto, T. Moro, K. Saiga, M. Hashimoto, H. Ito, H. Kawaguchi, Y. Takatori, K. Ishihara, Biomimetic hydration lubrication with various polyelectrolyte layers on cross-linked polyethylene orthopedic bearing materials, Biomaterials 33 (2012) 4451–4459.
[4] M.X. Tang, C. Chen, J.R. Zhu, H.R. Allcock, C.A. Siedlecki, L.C. Xu, Inhibition of bacterial adhesion and biofilm formation by a textured fluorinated alkoxyphosphazene surface, Bioact. Mater 6 (2021) 447–459.
[5] Y.C. Su, I. Cockerill, Y.F. Zheng, L.P. Tang, Y.X. Qin, D.H. Zhu, Biofunctionalization of metallic implants by calcium phosphate coatings, Bioact. Mater 4 (2019) 196–206.
[6] S.P. Singh, Y.L. Li, A. Be'er, Y. Oren, J.M. Tour, C.J. Arnusch, Laser-induced graphene layers and electrodes prevents microbial fouling and exerts antimicrobial action, ACS Appl. Mater. Interfaces 9 (2017) 18238–18247.
[7] L.B. Huang, S.Y. Xu, Z.Y. Wang, K. Xue, J.J. Su, Y. Song, S.J. Chen, C.L. Zhu, B. Z. Tang, R.Q. Ye, Self-reporting and photothermally enhanced rapid bacterial killing on a laser-induced graphene mask, ACS Nano 14 (2020) 12045–12053.
[8] J. Seror, L. Zhu, R. Goldberg, A.J. Day, J. Klein, Supramolecular synergy in the boundary lubrication of synovial joints, Nat. Commun. 6 (2015) 6497.
[9] G. Liu, Z. Liu, N. Li, X. Wang, F. Zhou, W. Liu, Hairy polyelectrolyte brushes-grafted thermosensitive microgels as artificial synovial fluid for simultaneous biomimetic lubrication and arthritis treatment, ACS Appl. Mater. Interfaces 6 (2014) 20452–20463.
[10] J. Klein, Hydration lubrication, Friction 1 (2013) 1–23.
[11] P.E. Milner, M. Parkes, J.L. Puetzer, R. Chapman, M.M. Stevens, P. Cann, J.R. T. Jeffers, A low friction, biphasic and boundary lubricating hydrogel for cartilage replacement,, Acta Biomater. 65 (2018) 102–111.
[12] B. Huang, L. Tan, X.M. Liu, J. Li, S.L. Wu, A facile fabrication of novel stuff with antibacterial property and osteogenic promotion utilizing red phosphorus and near-infrared light, Bioact, Materials 4 (2019) 17–21.
[13] X.L. Ji, Y.F. Yan, T. Sun, Q. Zhang, Y. Wang, M. Zhang, H.Y. Zhang, X. Zhao, Glucosamine sulphate-loaded distearoyl phosphocholine liposomes for osteoarthritis treatment: combination of sustained drug release and improved lubrication, Biomater. Sci. 7 (2019) 2716–2728.
[14] Y.X. Wang, Y.L. Sun, Y.H. Gu, H.Y Zhang, Articular cartilage-inspired surface functionalization for enhanced lubrication, Adv. Mater. Interfaces 6 (2019) 1900180.
[15] S. Renvert, C. Lindahl, H. Renvert, G.R. Persson, Clinical and microbiological analysis of subjects treated with branemark or astratech implants: a 7-year follow-up study, Clin. Oral Implants Res. 19 (2008) 342–347.
[16] A. Beaussart, M. Abellán-Flos, S. El-Kirat-Chatel, S.P. Vincent, Y.F. Dufreˆne, Force nanoscopy as a versatile platform for quantifying the activity of antiadhesion compounds targeting bacterial pathogens, Nano Lett. 16 (2016) 1299–1307.
[17] W.M. Dunne, Bacterial adhesion: seen any good biofilms lately? Clin. Microbiol. Rev. 15 (2002) 155–166.
[18] J. Palmer, S. Flint, J. Brooks, Bacterial cell attachment, the beginning of a biofilm, J. Ind. Microbiol. Biotechnol. 34 (2007) 577–588.
[19] M. Yamaguchi, Y. Terao, T. Ogawa, T. Takahashi, S. Hamada, S. Kawabata, Role of streptococcus sanguinis sortase A in bacterial colonization, Microb. Infect. 8 (2006) 2791–2796.
[20] C. Berne, A. Ducret, G.G. Hardy, Y.V. Brun, Adhesins involved in attachment to abiotic surfaces by gram-negative bacteria, Microbiol. Spectr. 3 (2015). MB-0018.
[21] C. Berne, C.K. Ellison, A. Ducret, Y.V. Brun, Bacterial adhesion at the single-cell level, Nat. Rev. Microbiol. 16 (2018) 616–627.
[22] S. Chen, J. Zheng, L. Li, S. Jiang, Strong resistance of phosphorylcholine self-assembled monolayers to protein adsorption: insights into nonfouling properties of zwitterionic materials, J. Am. Chem. Soc. 127 (2005) 14473–14478.
[23] H.S. Sundaram, X. Han, A.K. Nowinski, J.R. Ella-Menye, C. Wimbish, P. Marek, K. Senecal, S.Y. Jiang, One-step dip coating of zwitterionic sulfobetaine polymers

on hydrophobic and hydrophilic surfaces, ACS Appl. Mater. Interfaces 6 (2014) 6664–6671.
[24] F. Qi, Y. Qian, N. Shao, R. Zhou, S. Zhang, Z. Lu, M. Zhou, J. Xie, T. Wei, Q. Yu, R. Liu, Practical preparation of infection-resistant biomedical surfaces from antimicrobial β-peptide polymers, ACS Appl. Mater. Interfaces 11 (2019) 18907–18913.
[25] T. Wei, Q. Yu, H. Chen, Responsive and synergistic antibacterial coatings: fighting against bacteria in a smart and effective way, Adv, Healthcare Mater (2019) 1801381.
[26] Y.X. Qian, F. Qi, Q. Chen, Q. Zhang, Z.Q. Qiao, S. Zhang, T. Wei, Q. Yu, S. Yu, Z. W. Mao, C.Y. Gao, Y.R. Ding, Y.Y. Cheng, C.Y. Jin, H.X. Xie, R.H. Liu, Surface modified with a host defense peptide-mimicking β-peptide polymer kills bacteria on contact with high efficacy, ACS Appl. Mater. Interfaces 10 (2018) 15395–15400.
[27] Y. Han, S.Z. Liu, Y.L. Sun, Y.H. Gu, H.Y. Zhang, Bioinspired surface functionalization of titanium for enhanced lubrication and sustained drug release, Langmuir 35 (2019) 6735–6741.
[28] L. Cheng, Y. Wang, G. Sun, S.Z. Wen, L.F. Deng, H.Y. Zhang, W.G. Cui, Hydration-enhanced lubricating electrospun nanofibrous membranes prevent tissue adhesion, Research (2020) 4907185.
[29] S.Z. Liu, Q. Zhang, Y. Han, Y.L. Sun, Y.F. Zhang, H.Y. Zhang, Bioinspired surface functionalization of titanium alloy for enhanced lubrication and bacterial resistance, Langmuir 35 (2019) 13189–13195.
[30] M. Li, X.M. Liu, Z.Q. Xu, K.W.K. Yeung, S.L. Wu, Dopamine modified organic–inorganic hybrid coating for antimicrobial and osteogenesis, ACS Appl. Mater. Interfaces 8 (2016) 33972–33981.
[31] Q. Wei, X. Liu, Q. Yue, S. Ma, F. Zhou, Mussel-inspired one-step fabrication of ultralow-friction coatings on diverse biomaterial surfaces, Langmuir 35 (2019) 8068–8075.
[32] Z. Yang, X. Zhao, R. Hao, Q. Tu, X. Tian, Y. Xiao, K. Xiong, M. Wang, Y. Feng, N. Huang, G. Pan, Bioclickable and mussel adhesive peptide mimics for engineering vascular stent surfaces, Proc. Natl. Acad. Sci. U. S. A 117 (2020) 16127–16137.
[33] H. Ye, M. Han, R. Huang, T.A. Schmidt, W. Qi, Z. He, L.L. Martin, G.D. Jay, R. Su, G.W. Greene, Interactions between lubricin and hyaluronic acid synergistically enhance antiadhesive properties, ACS Appl. Mater. Interfaces 11 (2019) 18090–18102.
[34] L. Gong, L. Xiang, J. Zhang, L. Han, J. Wang, X. Wang, J. Liu, B. Yan, H.B. Zeng, Interaction mechanisms of zwitterions with opposite dipoles in aqueous solutions, Langmuir 35 (2019) 2842–2853.
[35] C. Wang, J. Hou, H.C. Mei, H.Y. Busscher, J. Rena, Emergent properties in streptococcus mutans biofilms are controlled through adhesion force sensing by initial colonizers, ASM mBio 10 (2019) e01908–e01919.
[36] C. Feuillie, C. Valotteau, L. Makart, A. Gillis, J. Mahillon, Y.F. Dufrêne, Bacterial sexuality at the nanoscale, Nano Lett. 18 (2018) 5821–5826.
[37] O.C.J. Van, Acid-base interfacial interactions in aqueous media, Colloids and Surfaces A: Physicochem, Eng. Aspects 78 (1993) 1–49.
[38] G.W. Greene, L.L. Martin, R.F. Tabor, A. Michalczyk, L.M. Ackland, R. Horn, Lubricin: a versatile, biological anti-adhesive with properties comparable to polyethylene glycol, Biomaterials 53 (2015) 127–136.
[39] C.P. Green, H. Lioe, J. Cleveland, R. Proksch, P. Mulvaney, J.E. Sader, Normal and torsional spring constants of atomic force microscope cantilevers, Rev. Sci. Instrum. 75 (2004) 988–1996.
[40] M. Varenberg, I. Etsion, G. Halperin, An improved wedge calibration method for lateral force in atomic force microscopy, Rev. Sci. Instrum. 74 (2003) 3362–3367.
[41] D.R. Dreyer, D.J. Miller, B.D. Freeman, D.R. Paul, C.W. Bielawski, Elucidating the structure of poly (dopamine), Langmuir 28 (2012) 6428–6435.
[42] H.W. Kim, B.D. McCloskey, T.H. Choi, C. Lee, M.J. Kim, B.D. Freeman, H.B. Park, Oxygen concentration control of dopamine-induced high uniformity surface coating chemistry, ACS Appl. Mater. Interfaces 5 (2013) 233–238.
[43] S. Hong, Y. Wang, S.Y. Park, H. Lee, Progressive fuzzy cation-π assembly of biological catecholamines, Sci. Adv 4 (2018) eaat7457.
[44] S. Hong, Y.S. Na, S. Choi, I.T. Song, W.Y. Kim, H. Lee, Non-covalent self-assembly and covalent polymerization co-contribute to polydopamine formation, Adv. Funct. Mater. 22 (2012) 4711–4717.
[45] L. Han, L. Xiang, J. Zhang, J. Chen, J. Liu, B. Yan, H.B. Zeng, Biomimetic lubrication and surface interactions of dopamine-assisted zwitterionic polyelectrolyte coatings, Langmuir 34 (2018) 11593–11601.
[46] M. Tanaka, S. Kobayashi, D. Murakami, F. Aratsu, A. Kashiwazaki, T. Hoshiba, K. Fukushima, Design of polymeric biomaterials: the “intermediate water concept”, Bull. Chem. Soc. Jpn. 92 (2019) 2043–2057.
[47] Y. Kaibara, K. Sugata, M. Tachiki, H. Umezawa, H. Kawarada, Control wettability of the hydrogen-terminated diamond surface and the oxidized diamond surface using an atomic force microscope, Diam. Relat. Mater. 12 (2003) 560–564.
[48] G.B. Kaggwa, P.C. Nalam, J.I. Kilpatrick, N.D. Spencer, S.P. Jarvis, Impact of hydrophilic/hydrophobic surface chemistry on hydration forces in the absence of confinement, Langmuir 28 (2012) 6589–6594.
[49] A. Beaussart, S.E.K. Chatel, R.M.A. Sullan, D. Alsteens, P. Herman, Quantifying the forces guiding microbial cell adhesion using single-cell force spectroscopy, Nat. Protoc. 9 (2014) 1049–1055.
[50] H. Lee, B.P. Lee, P.B. Messersmith, A reversible wet/dry adhesive inspired by mussels and geckos,, Nature 448 (2007) 338–341.